NATURAL GAS CONVERSION V
Studies in Surface Science and Catalysis, Vol. 119
A. Parmaliana et al. (Editors)

Non-oxidative catalytic conversion of methane with continuous hydrogen removal

Richard W. Borry III, Eric C. Lu, Young-Ho Kim*, and Enrique Iglesia

Materials Sciences Division, E.O. Lawrence Berkeley National Laboratory and
Department of Chemical Engineering, University of California, Berkeley CA 94720, USA

Simulations predict maximum C_2-C_{10} yields of 14% for both homogeneous and surface-initiated CH_4 pyrolysis at 1038 K. Yields are limited by thermodynamics, kinetic inhibition by H_2, and carbon formation. Continuous H_2 removal from the system can overcome these constraints and increase maximum predicted yields to 88%. CH_4 pyrolysis experiments at 950 K on 4 wt% Mo/H-ZSM5 achieves near-equilibrium conversions (10-12%) with >90% C_2-C_{10} selectivity by catalyzing both C_2H_4 formation from CH_4 (on MoO_xC_y) and C_2H_4 aromatization (on H^+), while restricting chain growth to benzene and naphthalene. An H-transport membrane reactor of dense $SrZr_{0.95}Y_{0.05}O_3$ thin (10-100 μm) films can be used to overcome these thermodynamic constraints. Self-supporting, thick (1000 μm) disks were prepared via combustion synthesis methods, which form denser membranes than powders formed via co-precipitation. Membrane reactor experiments using thick $SrZr_{0.95}Y_{0.05}O_3$ disks had H-transport rates insufficient to affect CH_4 pyrolysis reactions.

1. INTRODUCTION

The direct conversion of methane to fuels and petrochemicals remains a formidable challenge. Unrestricted chain growth during endothermic pyrolysis leads to undesired carbon and polynuclear aromatics. [1] Oxidative methane coupling avoids thermodynamic constraints by kinetically coupling C-H bond activation with removal of hydrogen via oxidation with O_2. These reactions, however, are unselective and lead to high CO and CO_2 yields. [2, 3] C-H bond activation and hydrogen removal steps can also be coupled by transporting hydrogen atoms across a dense ceramic membrane. This approach preserves the stoichiometry of oxidative coupling without direct contact between CH_4 and O_2 and allows the use of air as the oxidant. Electrochemical attempts to implement this approach have not led to practical yields, because of electrical and oxygen anion conductivity in $SrCe_{0.95}Yb_{0.05}O_3$ conductors and because of carbon deposition at electrodes. [4, 5] In the non-electrochemical approach proposed here (Figure 1), catalytic methane pyrolysis on Mo/H-ZSM5 forms C_{2+} hydrocarbons and H_2 on one side, H-atoms are transported across a dense oxide film, and reacted with air on the other side. Active Mo/H-ZSM5 catalysts allow this system to operate below 973 K, where homogeneous carbon formation is minimal. Here, we describe a rigorous analysis of reactor behavior using detailed kinetic-transport models, the characterization of the structural requirements and pathways for methane pyrolysis on Mo/H-ZSM5, and the synthesis and evaluation of proton conductors of $SrZr_{0.95}Y_{0.05}O_3$ composition.

* permanent address: Kunsan National University, Kunsan, Chonbuk 573-701, Korea

2. METHODS

2.1. Simulation of membrane reactors

A gas-phase kinetic model with 65 elementary steps involving 29 species describes accurately pyrolysis rates and selectivity below 1100 K, including the formation of C_{10+} hydrocarbons. [6] Surface reactions include CH_4 conversion to methyl radicals, recombination of H-atoms to give H_2, and transport of H atoms across the membrane. Methyl radical formation rates were estimated using linear free energy relations between C-H bond activation rates and O-H bond energies and O-H bond strengths in MoO_x-H. Reported diffusivities for $SrZr_{0.95}Y_{0.05}O_3$ were used to calculate hydrogen transport rates. [7] Molecules larger than naphthalene were assumed to form solid carbon.

Figure 1. CH_4 aromatization with hydrogen removal

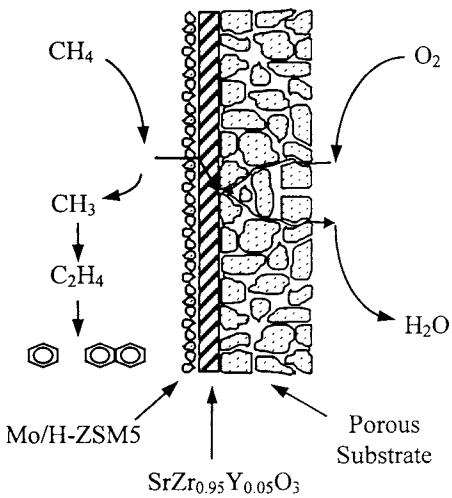

2.2. Mo/H-ZSM5 catalysts for methane pyrolysis

Mo/H-ZSM5 was prepared from physical mixtures of MoO_3 (Johnson Matthey, 99.5% purity) and H-ZSM5 (Zeochem, Si:Al=14.5). The effects of oxidation pre-treatment on catalyst structure and performance were examined using MoO_3/H-ZSM5 mixtures (0.3 g, 0-8 wt% Mo) dried at 623 K for 24 h in 20% O_2/Ar (100 cm^3/min). Samples were heated at 10 K/min to 973 K and H_2O evolution was measured by mass spectrometry (Leybold Inficon, model THP-TS200), using Ar as an internal standard. Samples were held at 973 K for 0.5 h, then cooled to 300 K. The number of exchangeable H atoms (mainly Bronsted acid sites) in treated MoO_3/H-ZSM5 samples was obtained by heating these samples from 300 K to 973 K (10 K/min) in 5% D_2/Ar (100 cm^3/min) and measuring the evolution of HD and H_2 by mass spectrometry. [8]

Catalytic CH_4 reactions were carried out at 950 K in a tubular reactor with plug-flow hydrodynamics (1.0 g, 25 cm^3/min, 1:1 CH_4/Ar, 1.08 bar). Product streams were analyzed on-line using heated transfer lines (400 K) and gas chromatography {HP6890 GC; Carboxen 1000 packed column (3.2 mm x 2 m, Supelco) with thermal conductivity detector and HP-1 capillary column (0.32 mm x 50 m, Hewlett-Packard) with flame ionization detector}. Catalysts were treated in 20% O_2/He (100 cm^3/min) at 950 K for 2 h before catalytic reactions. Selectivities are reported on a carbon basis, as the percentage of the converted CH_4 appearing as a given product, using Ar as an internal standard in order to ensure accurate mass balances. The carbon missing within the measured products (1-10%) is treated as solid carbon in reporting yields.

2.3. Membrane materials and synthesis methods

Dense $SrZr_{0.95}Y_{0.05}O_3$ membranes can transport hydrogen with perfect selectivity at 600-1000 K. [9] $SrZr_{0.95}Y_{0.05}O_3$ powders were prepared by co-precipitation of metal hydroxides (Y, Zr) or carbonate (Sr) at a pH of 9 from an aqueous solution of the metal nitrates using NH_4OH and $(NH_4)_2CO_3$. The perovskite structure was detected by X-ray diffraction after air treatment at 1223 K. Membrane precursor powders were also prepared using glycine-nitrate [10] and

glycolate [11] combustion methods, which result in smaller and easier-to-sinter particles with perovskite structure after oxidation at 1223 K. Powders were pressed into disks (25 mm dia. x 1.5 mm) and densified at 1823 K for 4 h in flowing air. This procedure led to smaller disks (16 mm dia. x 1 mm) with densities of 85-100% of the skeletal $SrZrO_3$ density. Disk densities were obtained by weighing and measuring with calipers. Powder surface areas were measured by N_2 physisorption at 77 K using the BET method (Quantachrome Autosorb-6).

3. RESULTS AND DISCUSSION

3.1. Simulation of membrane reactors

The activation of a C-H bond in CH_4 to form CH_3 and H radicals limits homogeneous pyrolysis rates and initiates a sequence of chain growth reactions. [12] The major stable molecular products are ethylene, benzene, and naphthalene at 823-1073 K. For this discussion, the reaction pathways can be simplified without loss of accuracy as:

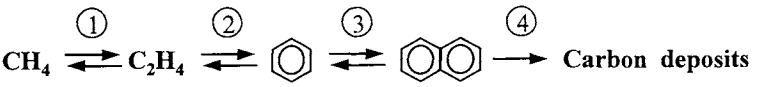

Reverse rates are important even at low CH_4 conversion (<5%), because of thermodynamic limitations (23% equilibrium conversion to C_2-C_{10} at 1038 K) and of the large amount of H_2 produced in sequential dehydrogenation steps.

Detailed simulations of CH_4 pyrolysis at 1038 K lead to the results in Figure 2. The maximum C_2-C_{10} yield is 14% for homogeneous reactions and does not change when a faster heterogeneous methyl radical generation function is added. This reflects the sequential nature of the reaction scheme above and of the full reaction mechanism. An increase in the rate of methyl radical formation leads to a faster equilibration of step 1 (limited to 8% conversion at

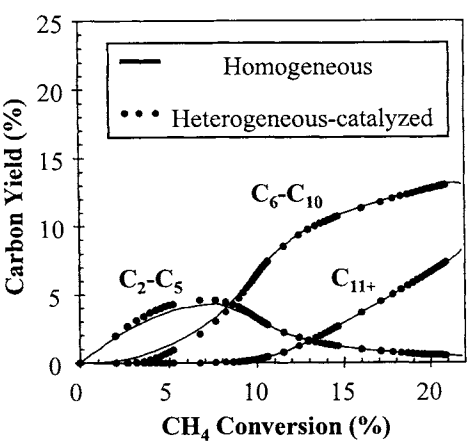

Figure 2. Simulation of CH_4 pyrolysis without H-removal (1038 K, 0.59 bar)

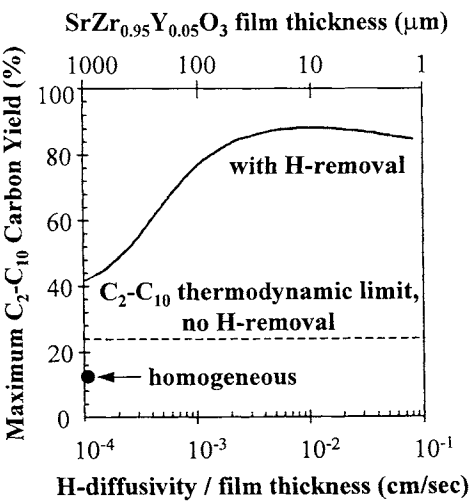

Figure 3. Effect of H-removal rate on CH_4 pyrolysis simulation (1038 K, 0.59 bar)

1038 K) and ethylene conversion to aromatics (step 2) becomes rate-limiting. Therefore, surface-initiated CH_4 reactions do not influence product selectivity above 10% CH_4 conversion, because homogeneous chain-growth (steps 2-4) determines the product distribution in the simulations.

Figure 3 shows the simulated effect of hydrogen removal on CH_4 pyrolysis yields. Removal of hydrogen at rates expected for a $SrZr_{0.95}Y_{0.05}O_3$ membrane of 1.0 mm thickness leads to maximum C_2-C_{10} yields of about 42% (at 85% CH_4 conversion). Higher conversions achieved by increasing residence times lead to lower C_2-C_{10} yields (<25%), because intermediate C_2-C_{10} products convert to coke precursors via slower chain-growth reactions (step 4). Thinner membrane films (5-50 μm) increase the rate of H removal without affecting the rate of carbon formation via chain-growth reactions and lead to maximum C_2-C_{10} yields near 90%.

Simulations also show that gas-phase CH_4 pyrolysis with continuous hydrogen removal leads to high C_2-C_{10} yields only at low temperature (<1000 K), above which unselective homogeneous pathways lead preferentially to carbon. Below 1000 K, achieving near-equilibrium CH_4 conversion within practical residence times requires a catalyst; this catalyst must restrict chain growth in order for yields to exceed those in homogeneous reactions and must also be stable at the severe reducing/carburizing conditions of CH_4 pyrolysis. H_2 transport rates must approach those of CH_4 reactions in order to maintain low H_2 concentrations, because H_2 inhibits CH_4 conversion. In addition, membrane materials must not reduce or carburize during operation.

3.2. Chain-limiting catalytic pyrolysis of methane on Mo/H-ZSM5

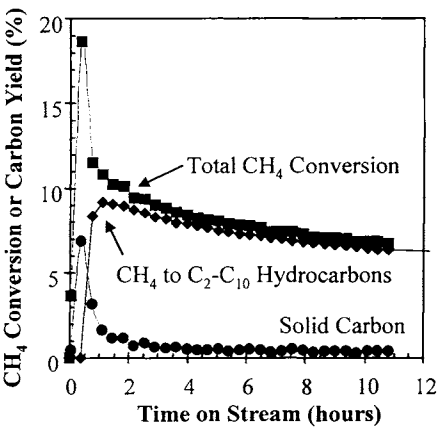

Figure 4. CH_4 pyrolysis on 4 wt% Mo/H-ZSM5 at 950 K

Recent studies have shown that Mo/H-ZSM5 restricts chain growth, increases reaction rates, and leads to CH_4 pyrolysis below 1000 K with low selectivity to carbon. [13, 14] Thermodynamic constraints, however, limit benzene yields to about 12% at 973 K. Our catalytic data (Figure 4) confirm these results using catalysts prepared via simple exchange of Mo^{+6} from MoO_3 onto H-ZSM5 by surface and gas-phase transport.

Mo/H-ZSM5 (4 wt% Mo) forms CO_2, CO, H_2O and carbon during initial contact with CH_4 at 950 K, as Mo^{+6} cations are converted to oxycarbide species (MoO_xC_y) that activate CH_4. Steady-state CH_4 conversions (9-11% at 750 cm^3 CH_4/g cat-h) and benzene selectivities (75%) are reached after 1 h. Deactivation decreases CH_4 pyrolysis rates (to 6% conversion after 40 h), but treatment in 20% H_2/He at 950 K restores initial rates and selectivities, without the activation period observed on fresh catalysts. Regeneration by temperature-programmed oxidation (400→950 K, 5 K/min) restores both initial induction periods and steady-state reaction rates.

Mo/H-ZSM5 appears to satisfy the requirements for low-temperature CH_4 activation catalysts suggested by our simulations of membrane reactors. Unfavorable thermodynamics for endothermic methane pyrolysis, however, preclude rate increases by further catalyst

modifications. Conversions greater than ~10% will require higher temperatures, lower methane pressure, or the continuous removal of one of the products during reaction. (Table 1)

Table 1. Thermodynamic equilibrium calculations for CH_4 conversion to C_2-C_{10} (950 K)

CH_4 pressure (bar)	1.0	0.05	1.0	1.0	1.0
H removal (%)	0	0	25	50	75
CH_4 conversion (%)	10.4	31.3	38.1	66.4	94.7

3.3. Structure and function of Mo cations in Mo/H-ZSM5

Pyrolysis rates on Mo/H-ZSM5 prepared by solid-state reaction of MoO_3/H-ZSM5 mixtures are similar to those on samples prepared via impregnation of H-ZSM5 with ammonium heptamolybdate. [13] During air oxidation of either sample, we expect isolated MoO_x species to move into the ZSM5 pore structure and exchange with H atoms located at framework acid sites. The rate of surface migration of MoO_x species into H-ZSM5 channels becomes significant above the Tammann temperature (534 K) [15] and gas-phase transport occurs above 623 K [16].

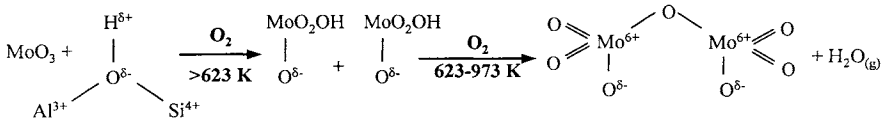

The number of H_2O molecules desorbed during heating in air corresponds to the number of protons exchanged by migration of MoO_x to exchange sites in H-ZSM5. (Figure 5, slope = 1.07 H/Mo) Also, the number of remaining H acid sites obtained by isotopic exchange of D_2 with surface OH groups in the zeolite decreases linearly as Mo concentration increases. (Figure 6a, slope = -1.02 H/Mo) Thus, one H^+ is lost from H-ZSM5 for each Mo exchanged, up to a Mo concentration of 5.1 wt% Mo, beyond which surface O-H groups disappear. Higher Mo concentrations lead to sublimation of the excess MoO_x. The stoichiometries shown by the data in Figures 5 and 6a, charge balance requirements, and preliminary X-ray absorption and NMR results [17] are consistent with isolated $(Mo_2O_5)^{2+}$ dimers interacting with two cation exchange

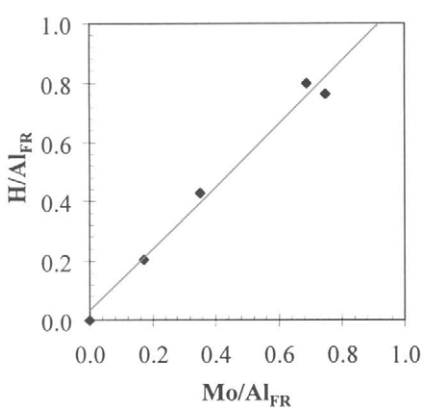

Figure 5. Number of H per framework Al (Al_{FR}) desorbed as H_2O during oxidation of MoO_3/H-ZSM5 mixtures

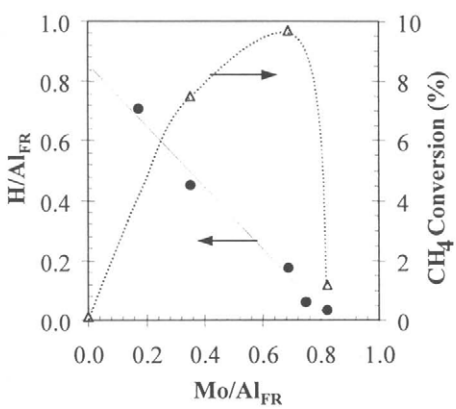

Figure 6. a) Number of exchangeable H per Al remaining on oxidized MoO_3/H-ZSM5 samples b) CH_4 conversion at 950 K vs. Mo loading

sites, which convert to MoO_xC_y during CH_4 reactions. CH_4 conversion rates reach a maximum value at intermediate Mo concentrations (Figure 6b), suggesting a requirement for both Mo species and H^+ in CH_4 conversion pathways.

3.4. Methane activation and acid-catalyzed oligomerization reactions

Figure 7 shows product selectivities on 4 wt% Mo/H-ZSM5 at 950 K as conversion changes by varying space velocity (150-1500 cm^3/g cat-h), catalyst loading (0.5-1.0 g), or the extent of deactivation (1-96 h on stream). The coincidence of deactivation and residence time results show that deactivation occurs by loss of active sites without modification of intrinsic site chemistry. These selectivity/conversion curves demonstrate that CH_4 reacts sequentially to form C_2H_4 as the initial reactive product, C_6H_6 as a secondary product, and naphthalene as the kinetic end point (except for its slow conversion to carbon). Earlier studies [13, 14] also suggested sequential pathways involving CH_4 activation on Mo sites to produce CH_3 radicals, C_2H_6, and then C_2H_4 via homogeneous pathways, followed by acid-catalyzed chain growth reactions of C_2H_4 within shape-selective ZSM5 channels (~5.5 Å diameter), which limit the size of polymeric products. C_2H_4 reacts via oligomerization and cyclization reactions on residual protons in Mo/H-ZSM5 to form single-ring aromatics and naphthalene. The instantaneous removal of C_2H_4 (via aromatization) removes thermodynamic and kinetic constraints that limit CH_4 to C_2H_4 reactions to low conversions (3.8 %) at 950 K.

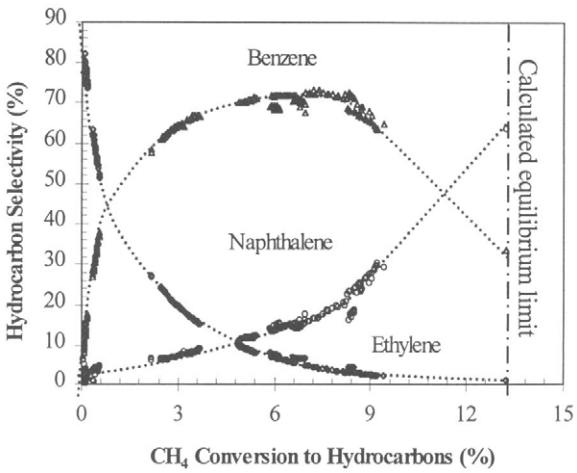

Figure 7. CH_4 conversion vs. product selectivity at different space velocities and levels of deactivation (950 K, 0.5-1.0 g 4% Mo/H-ZSM5, 5-50 cm^3/min 1:1 CH_4/Ar)

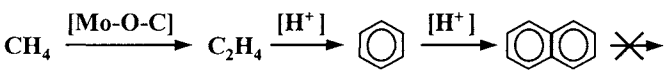

The effect of the relative numbers of $Mo^{\delta+}$ and H^+ sites on CH_4 conversion (Figure 6b) confirms the bifunctional nature of reaction pathways. CH_4 conversion rates increase as Mo concentration increases (0-4 wt% Mo), because the initial formation of C_2H_4 limits overall rates as long as H^+ sites are available to convert C_2H_4 into more stable aromatics. When H^+ sites disappear at Mo concentrations above 4 wt%, CH_4 conversion decreases sharply, because it is limited by the unfavorable equilibrium of C_2H_4 formation.

3.5. Synthesis and characterization of membrane materials

Metal membranes (Pd, Pd/Ag) cannot be used in our proposed scheme (Figure 1), because they cause rapid carbon formation during CH_4 pyrolysis. [18] $SrCe_{0.95}Yb_{0.05}O_3$ proton-transport membranes exhibit oxide ion mobility at 1023 K [5] and lose oxygen in reducing environments.

$SrZr_{0.95}Y_{0.05}O_3$ has H-diffusivities similar to those in $SrCe_{0.95}Yb_{0.05}O_3$ [7], but remains stable in reducing environments. [19] Our simulation results (section 3.1) show that practical membranes must transport hydrogen at rates comparable to reaction rates. These constraints translate into a requirement for the synthesis of thin (10-100 μm) films of $SrZr_{0.95}Y_{0.05}O_3$ perovskite.

$SrZr_{0.95}Y_{0.05}O_3$ is difficult to form into dense membranes. [20] The synthesis of dense ceramics depends critically on the size and uniformity of the powders used to form the compressed porous structure ("green" body) that must then be sintered into disks or films with densities above 95% of the skeletal perovskite density. Small crystallites of uniform size favor desired densification processes, which form gas-tight structures, over sintering processes that form large pores and weak structures with low bulk density. [21] Table 2 shows some representative properties of $SrZr_{0.95}Y_{0.05}O_3$ powders prepared by three different methods. Combustion synthesis methods lead to loose powders with low density and smaller crystallites with higher surface area, because the rapid exothermic decomposition of metal nitrate/organic precursors cause the formation of a large number of isolated nuclei during expansion and quenching of the reacting mixture. Individual nuclei grow by consuming reactants within a surrounding diffusion radius without significant agglomeration of crystallites.

Table 2
Properties of $SrZr_{0.95}Y_{0.05}O_3$ powders before densification into H-transport membranes

Method	"Loose" powder density (g/cm^3)	BET surface area (m^2/g)	"Green" disk density (% of $SrZrO_3$ theoretical)
Co-precipitation	1.34	4.79	44
Glycine-nitrate	0.016	19.1	48
Ammonium glycolate	0.070	12.3	51

The packed density of "green" disks after isostatic compression at 138 MPa is similar for the three synthesis methods. (44-51%, Table 2) After sintering at 1673-1923 K for 4 h, however, materials prepared by combustion methods lead to disks with much higher densities (Figure 8). Disks from co-precipitated powders did not densify at all at these conditions. Even after mechanical grinding and hydrostatic compression at 1240 MPa, their bulk densities were much lower than those of powders prepared by glycolate and glycine-nitrate combustion methods.

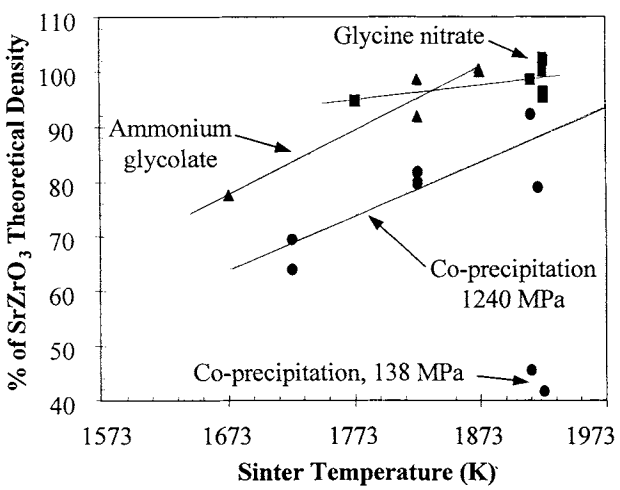

Figure 8. Effect of sintering temperature on final membrane density for three $SrZr_{0.95}Y_{0.05}O_3$ powders

$SrZr_{0.95}Y_{0.05}O_3$ disks (0.9-1.2 mm thick) with >95% theoretical density were sealed to the end of a 19 mm O.D. alumina tube using a ceramic paste (Aremco Ceramabond 571). Mo/H-ZSM5 (0.5 g, 4 wt% Mo) was placed on the methane side of the disk, while the opposite side was left

exposed to air. This membrane reactor was heated at 0.5 K/min to 950 K, leak-tested using He, and exposed to CH_4 (150 cm^3 CH_4/g cat-h). CH_4 conversion rates and product selectivity were similar to those measured in conventional tests (without hydrogen removal). The estimated H_2 transport rate at 950 K for a $SrZr_{0.95}Y_{0.05}O_3$ disk with 1.5 cm^2 area is 44 μmol/h, which is significantly lower than the measured rate of H_2 production from CH_4 (930 μmol/h). Thus, less than 5% of the H_2 formed was removed and reaction rate enhancements were not detectable. These initial experiments and the simulation results (section 3.1) show that H_2 removal rates must increase by about a factor of 20, either by increasing the surface area or decreasing the thickness of the membrane. The latter approach can be implemented by sequential spin coating of viscous $SrZr_{0.95}Y_{0.05}O_3$ slurries onto porous Al_2O_3 or ZrO_2 supports. [22] The use of sequential coating/oxidation steps with powders formed via combustion methods has led to the synthesis of thin films with high densities, which are being tested in our membrane reactor.

4. ACKNOWLEDGEMENTS

The authors thank Drs. Anthony Dean and Sebastian Reyes of the Corporate Research Labs at Exxon Research and Engineering for some of the FORTRAN subroutines and kinetic and thermodynamic data used in the kinetic simulations. Richard Borry was supported by a National Science Foundation Fellowship. Dr. Young-Ho Kim was supported by the Korean Science and Engineering Foundation (KOSEF) during his sabbatical leave. Project funding was provided by the Federal Energy Technology Center (U.S. Department of Energy, contract DE-AC03-76SF00098) under the technical supervision of Dr. Daniel Driscoll.

REFERENCES

1. Chen, C.-J., M.H. Back, R.A. Back, *Can J Chem* **54** 3175 (1976)
2. Labinger, J.A., *Catal Lett* **1** 371 (1988)
3. Reyes, S.C., E. Iglesia, C.P. Kelkar, *Chem Engr Sci* **48** 2643 (1993)
4. Hamakawa, S., T. Hibino, H. Iwahara, *J Electrochem Soc* **140** 459 (1993)
5. Langguth, J., R. Dittmeyer, H. Hofmann, G. Tomandl, *Appl Catal A* **158** 287 (1997)
6. Borry, R.W., E. Iglesia, *Chem. Eng. Sci. (submitted for publication)* (1998)
7. Schober, T., J. Friedrich, J.B. Condon, *Solid State Ionics* **77** 175 (1995)
8. Biscardi, J.A., G.D. Meitzner, E. Iglesia, *J Catal (submitted for publication)* (1998)
9. Shin, S., Huang, H.H., Ishigame, M., Iwahara, H., *Solid State Ionics* **40/41** 910 (1990)
10. Chick, L.A., I.R. Pederson, G.D. Maupin, J.L. Bates, L.E. Thomas, G.J. Exarhos, *Mater Letters* **10** 6 (1990)
11. Soled, S.L., E. Iglesia, S. Miseo, B.A. DeRites, R.A. Fiato, *Top Catal* **2** 193 (1995)
12. Dean, A.M., *J Phys Chem* **94** 1432 (1990)
13. Wang, D., J.H. Lunsford, M.P. Rosynek, *Topics in Cat* **3** 289 (1996)
14. Solymosi, F., J. Cserenyi, A. Szoke, T. Bansagi, A. Oszko, *J Cat* **165** 150 (1997)
15. Satterfield, C.N., Heterogeneous Catalysis in Industrial Practice, (New York:McGraw-Hill, Inc.) 1991
16. Brewer, L., Molybdenum: Physico-chemical properties of its compounds and alloys, (Vienna:International Atomic Energy Agency) 1980
17. Borry, R.W., A. Huffsmith, G. Meitzner, J. Reimer, E. Iglesia, *(in preparation)* (1998)
18. Andersen, A., I.M. Dahl, K-J. Jens, E. Rytter, A. Slagtern, A. Solbakken, *Cat Today* **4** 389 (1989)
19. Yajima, T., H. Suzuki, T. Yogo, H. Iwahara, *Solid State Ionics* **51** 101 (1992)
20. Iwahara, H., T. Yajima, T. Hibino, K. Ozaki, H. Suzuki, *Solid State Ionics* **61** 65 (1993)
21. Rahaman, M.N., Ceramic Processing and Sintering, (New York:Marcel Dekker, Inc.) 1995
22. de Souza, S., S.J. Visco, L.C. De Jonghe, *Solid State Ionics* **98** 57 (1997)